Bai, Xueyin; Xu, Zhenyu; Zhang, Qiang; Li, Shisheng; Dai, Yunyun; Cui, Xiaoqi; Yoon, Hoon Hahn; Yao, Lide; Jiang, Hua; Du, Mingde; Zhang, Yi; Kauppinen, Esko I.; Sun, Zhipei

Molybdenum Disulfide/Double-Wall Carbon Nanotube Mixed-Dimensional Heterostructures

Published in:
Advanced Materials Interfaces

DOI:
10.1002/admi.202200193

Published: 04/05/2022

Document Version
Publisher's PDF, also known as Version of record

ADVANCED MATERIALS INTERFACES
www.advmatinterfaces.de

Molybdenum Disulfide/Double-Wall Carbon Nanotube Mixed-Dimensional Heterostructures

Xueyin Bai, Zhenyu Xu, Qiang Zhang,* Shisheng Li, Yunyun Dai, Xiaoqi Cui, Hoon Hahn Yoon, Lide Yao, Hua Jiang, Mingde Du, Yi Zhang, Esko I. Kauppinen, and Zhipei Sun**

Mixed-dimensional heterostructures which combine materials with different dimensions have emerged to expand the scope and functionality of van der Waals heterostructures. Here, a direct synthesis method of molybdenum disulfide/double-wall carbon nanotube (MoS_2/DWCNT) mixed-dimensional heterostructures by sulfurating a molten salt, Na_2MoO_4, on a substrate covered with a DWCNT film is reported. The synthesized heterostructures are comprehensively characterized and their stacking order is confirmed to be MoS_2 under the DWCNTs, although the DWCNT film is transferred on the substrate first. Moreover, field-effect transistors based on the heterostructure are fabricated for photodetection, and an abnormal negative photoresponse is discovered due to the strong carrier transfer in the mixed-dimensional heterostructures under light incidence. The MoS_2/DWCNT heterostructure results provide a new approach for the synthesis and applications of mixed-dimensional heterostructures.

1. Introduction

Recently, 2D layered materials have attracted significant interest because of the unique physical and chemical properties for numerous applications.[1] Further, different 2D materials can be stacked layer-by-layer to form van der Waals homo- or heterostructures that provide intriguing physical and chemical properties for the applications, such as energy storage, functional nano-devices, superconductors.[2,3] Very recently, the combination of 2D with other dimensional materials, in other words, mixed-dimensional heterostructures, have been demonstrated as a very promising and highly compatible platform for next-generation nanoelectronics and nanophotonics.[4–7]

Molybdenum disulfide (MoS_2) is one of the most interesting 2D materials mainly due to its semiconducting direct bandgap, making it a promising material for electronics, optoelectronics, and photonics.[8–10] Meanwhile, carbon nanotubes, one of the well-studied 1D materials, can provide a high conductivity and carrier mobility,[11,12] which makes them a perfect ally for a mixed-dimensional heterostructure with MoS_2. Indeed, some efforts have contributed to the MoS_2/carbon nanotube heterostructures. For example, heterostructures with MoS_2 and single-wall carbon nanotubes have been fabricated by dry transfer and make a vertical field-effect transistor which has three orders of magnitude increase in the gate modulation depth compared with that of the MoS_2/graphene devices.[13] The mixed-dimensional heterostructure devices could be used as thin-film transistors in active displays, but the demonstrated dry transfer is, obviously, not an ideal method for scalable production. To address this problem, the direct deposition of MoS_2 on single-wall carbon nanotubes by chemical vapor deposition (CVD) is developed. Transition metal oxides and sulfur are used as precursors to deposit MoS_2 or WS_2 on single-wall carbon nanotube films.[14] In this work, the mixed-dimensional heterostructure devices exhibit attractive electrical properties and excellent mechanical stability. However, the stacking order of mixed-dimensional heterostructures, which can provide a further understanding of the connection between heterostructures and electrodes, is neglected in the study.

Here, for the first time, we report a method for directly synthesizing MoS_2/double-wall carbon nanotube (DWCNT)

X. Bai, Y. Dai, X. Cui, H. H. Yoon, M. Du, Y. Zhang, Z. Sun
Department of Electronics and Nanoengineering
Aalto University
P. O. Box 13500, Aalto FI-00076, Finland
E-mail: xueyin.bai@aalto.fi; zhipei.sun@aalto.fi
Z. Xu, Q. Zhang, L. Yao, H. Jiang, E. I. Kauppinen
Department of Applied Physics
Aalto University
P. O. Box 13500, Aalto FI-00076, Finland
E-mail: qiang.zhang@aalto.fi
S. Li
International Center for Young Scientists (ICYS)
National Institute for Materials Science (NIMS)
Tsukuba 305-0044, Japan
Z. Sun
QTF Centre of Excellence
Department of Applied Physics
Aalto University
P. O. Box 13500, Aalto FI-00076, Finland

The ORCID identification number(s) for the author(s) of this article can be found under https://doi.org/10.1002/admi.202200193.

DOI: 10.1002/admi.202200193

mixed-dimensional heterostructures via a novel CVD mechanism, called vapor–liquid–solid (VLS) mechanism,[15–18] in which molten salts (such as Na_2MoO_4) are used as transition metal precursors to reduce the reaction temperature. The MoS_2 flakes synthesized with the DWCNTs are monolayer crystals and have a size of tens of micrometres. Further, with the cross-sectional high-resolution transmission electron microscopy (HR-TEM), the stacking order of MoS_2/DWCNT heterostructures is demonstrated to be MoS_2 flakes under the DWCNT film, although DWCNT film is transferred to the substrate first. To the best of our knowledge, the stacking order of synthesized MoS_2/carbon nanotube heterostructures is confirmed for the first time. We also fabricate symmetric and asymmetric transistors and measure their properties for photodetection, showing the possibility of using the mixed-dimensional heterostructures for photonic and optoelectronic applications.

2. Results and Discussion

The schematic illustration of the growth set-up is shown in **Figure 1**a. To synthesize the MoS_2/DWCNT heterostructures, a substrate with DWCNTs is needed. DWCNTs are synthesized by a floating catalyst CVD method, using methane as carbon sources, ferrocene as catalyst precursor, and sulfur as a promoter in the nitrogen atmosphere.[19] Then, a thin film of DWCNTs is collected by a membrane filter at ambient temperature and transferred to an *i*-propanol-rinsed pre-cleaned silicon substrate. The rinsing could increase the adhesion between DWCNTs and Si substrate and avoid the peeling-off in the next step. After spin-coated with 5 mg mL^{-1} Na_2MoO_4 aqueous solution, the substrate is put in the centre of the tube furnace (Figure 1a). Meanwhile, sulfur is loaded upstream with an individual heating tape. 100 sccm nitrogen is applied as the carrier gas. The substrate in the furnace is heated up to 700 °C with a ramping rate of 10 °C per minute and maintained for 10 min. The temperature of sulfur is fixed at 140 °C during the sulfuration. After the sulfuration, monolayer MoS_2 flakes form on the surface of a silicon substrate, thus shape into a MoS_2/DWCNT heterostructure. The scanning electron microscopy (SEM) images of synthesized MoS_2/DWCNT heterostructures are shown in Figure 1b,c, respectively, where the dark island-like flakes are MoS_2 and light fibres are DWCNTs. Figure 1d is a high-magnification SEM image, which shows that a synthesized MoS_2 flake is overlapping with DWCNTs, indicating that a MoS_2/DWCNT heterostructure is formed. It is worth noticing that the boundaries of MoS_2 are usually aligned with DWCNTs, which means the growth of MoS_2 is either impeded by DWCNTs or is extending along the DWCNTs. This phenomenon is believed to be caused by the special mechanism of the VLS method. During the heating, after Na_2MoO_4 melts and sulfur dissolves in the fusion, MoS_2 is grown with the extending of the liquid mixture.[15] It is easy to understand the expending of MoS_2 along the DWCNTs because the liquid precursor flows along the DWCNTs. For the impending, the abundant liquid mixture is able to overtop or permeate short barriers, such as DWCNTs here, but after several barriers, the amount of liquid mixture is too small to pass the last one, and the growth stops at the last barrier.

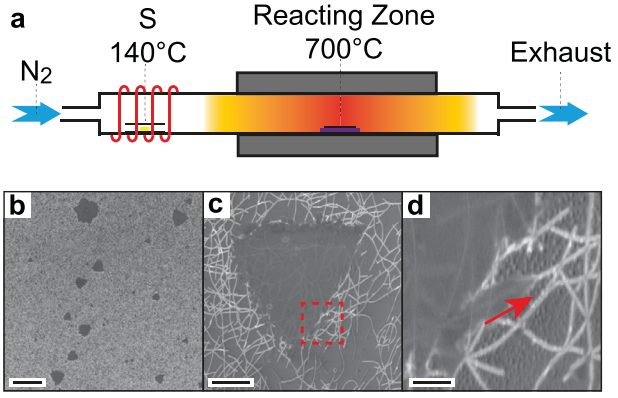

Figure 1. Schematic illustration of the growth setup and images of the MoS_2/DWCNT heterostructures. a) Schematic illustration of the CVD system. b) Scanning electron microscopy (SEM) image of MoS_2/DWCNT heterostructures (scale bar, 20 µm). c) High magnification SEM image of a MoS_2 flake (scale bar, 2 µm). d) Enlarged image of the marked area in (c) (scale bar, 400 nm).

To understand the cross-sectional structure of the MoS_2/DWCNT heterostructure, cross-sectional thin lamellae are prepared, which is then investigated with a high-resolution transmission electron microscope (HR-TEM). The lamellae for cross-sectional TEM are prepared with the focused ion beam technique. In brief, a layer of platinum with a thickness of ≈1 µm is first deposited on the target area to avoid the etching of MoS_2 and DWCNT from the ionic beam. Next, gallium ions are used to cleave the sample and obtain a lamella for TEM observing. **Figure 2**a shows the typical cross-sectional morphology of MoS_2 on the substrate. A clear atomic-thick layer is observed between the amorphous SiO_2 layer with a thickness of 285 nm and crystalline platinum particles deposited on Si substrate. This layer is confirmed to be a monolayer MoS_2 due to the layer distance (0.7 nm) and elementary composition measured at a multilayer part (see Figure S1, Supporting Information). Except for monolayer MoS_2 between SiO_2 and Pt, two-wall distorted concentric circles are observed on monolayer MoS_2, as shown in Figure 2b. Obviously, the two-wall circles are DWCNTs deformed by the pressure in the platinum depositing process. The height of the distorted concentric circles is ≈3 nm, corresponding to the height of DWCNTs measured by AFM (Figure S2, Supporting Information). Hence, the cross-sectional morphology of MoS_2/DWCNT heterostructure has confirmed that, although DWCNT film is first transferred on the substrate, MoS_2 synthesized by the VLS method is growing under the DWCNT film instead of

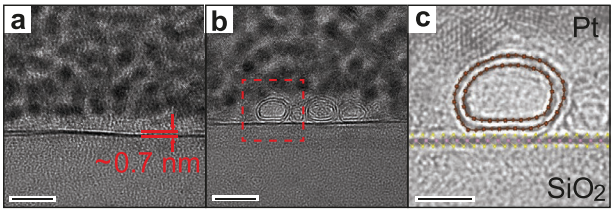

Figure 2. Cross-sectional HR-TEM images. a) Cross-sectional TEM image of a MoS_2 flake (scale bar, 5 nm). b) Cross-sectional TEM image of a MoS_2/DWCNT heterostructure (scale bar, 5 nm). c) Schematic illustration of the selected area in (b) (scale bar, 2 nm).

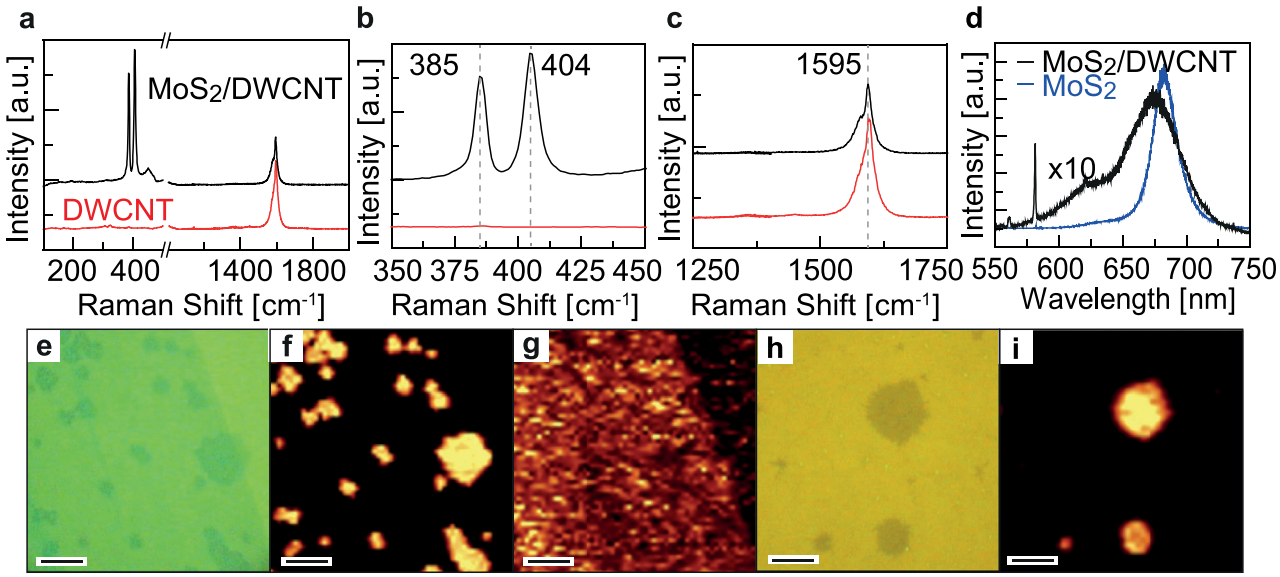

Figure 3. Optical characterizations of the MoS_2/DWCNT heterostructure. a) Raman spectra of the MoS_2/DWCNT heterostructure (black) and DWCNT film (red), respectively. b,c) Enlarged spectra of (a) in the specific ranges. d) Photoluminescence of the MoS_2/DWCNT heterostructure (×10 magnification, black) and a referenced MoS_2 flake (blue). e) Optical image of the MoS_2/DWCNT heterostructures (scale bar, 20 μm). f,g) Corresponding Raman intensity map of (e) at the Raman shift of ≈404 cm^{-1}, MoS_2 A_{1g} mode (f) and ≈1595 cm^{-1}, DWCNT G band (g), respectively (scale bar, 20 μm). h,i) Optical image and corresponding photoluminescence intensity map (i) of (h) at the wavelength of ≈672 nm (scale bar, 20 μm).

on the top of it. In other words, MoS_2 flakes are sandwiched between DWCNT films and substrates. The reason for no MoS_2 stacking on the DWCNTs might be the relatively uneven surface of the silicon substrate, which creates nanochannels between DWCNTs and the substrate. During the reaction, the molten salt permeates through these channels and conformally grows MoS_2 crystals. We notice in one cross-sectional TEM morphology the numbers of MoS_2 layers are different from one side to another side of the DWCNT, as shown in Figure S1, Supporting Information. Based on the VLS mechanism, more molten salts should form thicker layers, and different layers indicate the different amount of molten salts, certifying the molten salt permeates from one side to another side.

The MoS_2/DWCNT heterostructures are first characterized by Raman spectroscopy. **Figure 3**a shows the spectra measured from island-like flakes (MoS_2/DWCNT heterostructure, black) and background film (DWCNT, red), respectively. In the detailed Raman spectra, as shown in Figure 3b, two significant modes appear at ≈385 and ≈404 cm^{-1} which are the E_{2g} and A_{1g} modes of MoS_2, respectively. The wavenumber difference of the two modes is 19 cm^{-1}, indicating the flakes are monolayer MoS_2.[20] The thickness of island-like flakes around 0.9 nm measured by atomic force microscopy (AFM), as shown in Figure S2, Supporting Information, further confirms that the as-synthesized MoS_2 only has one layer. Both spectra in Figure 3c have a Raman mode at 1595 cm^{-1} which is the G band of DWCNTs, indicating both island-like MoS_2 flakes and DWCNT film are covered with DWCNTs. Besides, it is worth noting that no Raman mode is observed at approximated 1350 cm^{-1} which is the called D band of DWCNTs. Since the D band is referred to as the defect level in the carbon nanotubes,[7] no observation of D band indicates that no detectable defect is introduced to DWCNTs. In other words, DWCNTs preserve good quality, and no chemical doping is observed during the growth of MoS_2. Hence, it is confirmed that monolayer MoS_2 flakes are synthesized without sacrificing the quality of DWCNTs, and MoS_2/DWCNT heterostructures are formed. A Raman mapping of Figure 3e is also measured for investigating the uniformity of MoS_2/DWCNT heterostructures. Figure 3f,g is the maps of peak intensities at 404 and 1595 cm^{-1}, respectively. All the island-like flakes in Figure 3e are confirmed to be MoS_2 due to their strong signals at 404 cm^{-1} from Figure 3f. Meanwhile, Figure 3g offers evidence that the DWCNT film still covers the substrate after the growth of MoS_2. The Raman mapping indicates all MoS_2 flakes are combined with DWCNTs and form MoS_2/DWCNT heterostructure.

Due to its direct bandgap, monolayer MoS_2 has a strong photoluminance (PL) as the blue curve shown in Figure 3d. However, after being combined with DWCNTs, the intensity of PL is significantly weaker as the black curve shown in Figure 3d. The decreasing intensity is believed to be the exciton annihilation when semiconductor MoS_2 is contacting with metals, such as the metallic DWCNTs.[21] After absorbing exciting photons, the excited electrons in MoS_2 transit to the conduction band from the valence band. Due to the metallic properties of DWCNTs, the excited electrons transfer to DWCNTs instead of transiting back to the valence band and emitting photons, leading to an annihilated destruction of excitons. This contributes to a much weak PL in the mixed-dimensional heterostructure. Besides, the blue shift and the broad peak of the PL are considered due to the hole doping or introduced defects from DWCNTs.[22] The PL intensity map Figure 3i, indicates the uniformity of the flakes. Worth noting that no intensity change is observed from the reflection spectra and second-harmonic generation spectra (Figure S3, Supporting Information), indicating no detectable strong coupling interaction exists between MoS_2 and DWCNT in the heterostructure.

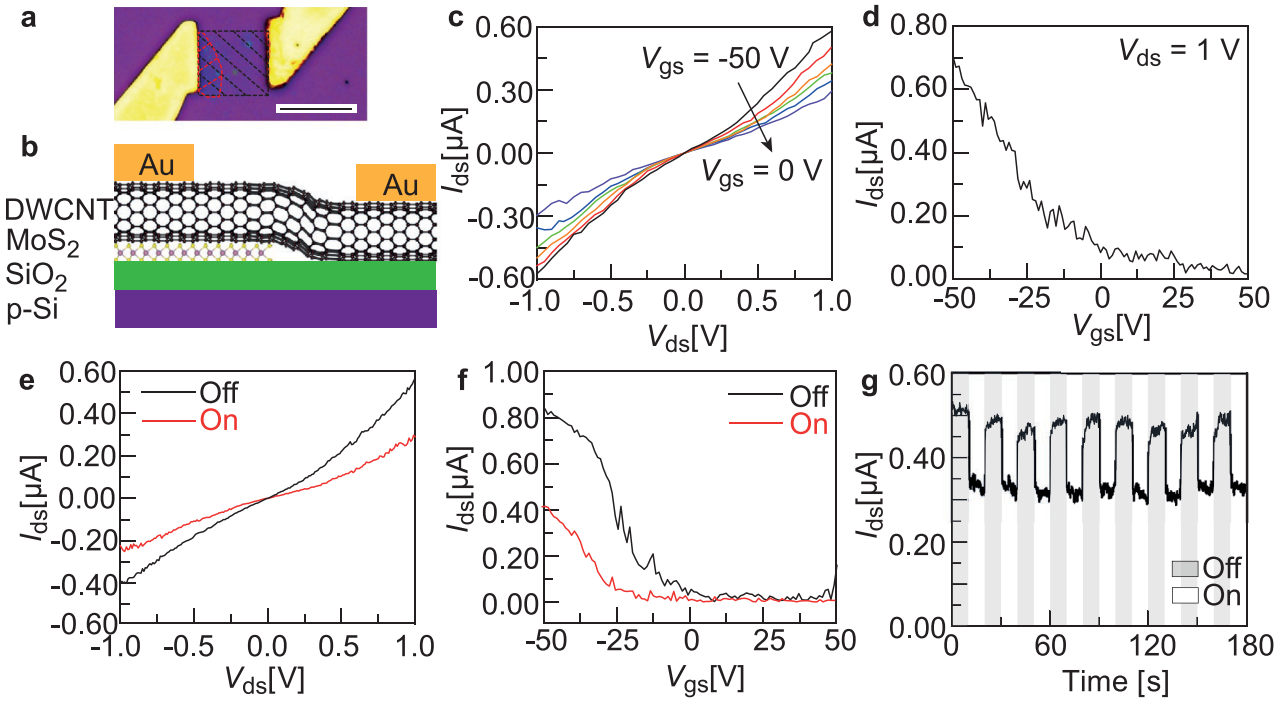

Figure 4. MoS_2/DWCNT heterostructures transistors. a) Optical image of a typical asymmetric transistor with the black part of DWCNT film and the red part of MoS_2 (scale bar, 10 μm). b) Schematic illustration of the asymmetric transistor. c) Output characteristics of the device in (a) at V_{gs} of 0 V (purple curve), −10 V (blue curve), −20 V (green curve), −30 V (orange curv00e), −40 V (red curve), and −50 V (black curve), respectively. d) transfer characteristics of the device in (a) at V_{ds} of 1 V. e,f) Output and transfer characteristics of the device in a without light (off, black curve) and with 0.1 mW light incidence power (on, red curve), respectively. g) Transient photoresponse of the device in (a) with a light duration of 10 s.

After confirming the structure of MoS_2/DWCNT heterostructures, asymmetric back-gated field-effect transistors (FETs) are fabricated to investigate their electrical and optoelectronic properties. A typical one shown in **Figure 4**a. The cross-sectional schematic of FETs is shown in Figure 4b, which clearly illustrates one electrode is contacted with MoS_2/DWCNT heterostructure while another one is on the DWCNT film. The typical output characteristics (I_{ds}–V_{ds}) at the gate voltage V_{gs} = 0–50 V and transfer characteristic (I_{ds}–V_{gs}) at V_{ds} = 1 V of the asymmetric transistor are shown in Figure 4c,d, respectively. The output characteristics exhibit non-linear relationships and non-rectifying behaviors, suggesting Schottky contacts are formed on each side of the MoS_2 channel.[23] I_{ds} increases from 0.15 to 0.6 μA when V_{gs} decreases from 0–50 V, indicating the gate modulation is, although very weak, existed, which is further proved by the transfer characteristic shown in Figure 4d. Transfer characteristic also indicates the DWCNT films are p-type semiconductors since a higher I_{ds} at V_{gs} = −50 V than at V_{gs} = 0 or 50 V. For comparison, symmetric devices are made with both electrodes contacted with the DWCNT film, and no MoS_2 is in the channel, as shown in Figure S4, Supporting Information. The symmetric transistor has an Ohmic contact between the source and drain electrodes and almost no gate-tunability, indicating the whole symmetric channel is metallic. In most of the published works,[13,24] the semiconductor properties of MoS_2/single-wall carbon nanotube heterostructures are considered from the p–n junction formed between p-type semiconducting single-wall carbon nanotube and n-type CVD MoS_2. However, in our research, the DWCNTs used are metallic without any chemical doping and will not act as p-type semiconductors. The metallic property of DWCNTs retains at the position without MoS_2 after the growth, which is confirmed by the Ohmic contacts of the symmetric transistors. Moreover, the stacking order in our heterostructure, MoS_2 under the DWCNTs, indicates both electrodes are contacted with DWCNTs directly, avoiding the formation of the p–n junction between MoS_2 and DWCNTs. Then, it is interesting to discover the reason for the formation of p-type semiconductors. The symmetric band structure of the metallic DWCNTs leads to efficient injection of both electrons and holes, rending both high performance n- and p-type semiconductors.[25] Meanwhile, when applying with high gate voltage, MoS_2 works as an n-type semiconductor which injects electrons to DWCNTs.[15,26] The injected electrons neutralize the holes in the DWCNTs, reduce the mobility and conductivity and finally leads the DWCNTs to be n-type semiconductors. Hence, the semiconducting properties of our MoS_2/DWCNT heterostructure are supposed to be explained as the holes neutralizing by the injecting electrons from the n-type MoS_2 at a high gate voltage.

Besides, the asymmetric transistors are applied as photodetectors. As shown in Figure 4e, an abnormal negative photoresponse occurs when a 514 nm laser with a power of 0.1 mW is shot on the device with V_{gs} = −20 V, while the symmetric device shows the normal positive photoresponse. This negative photoresponse later is confirmed to be existed in the whole gate voltage range from −50 to 0 V, as shown in Figure 4f. A transient

photoresponse on–off characteristic is shown in Figure 4g. The output current follows the switching status closely from the light pulses, confirming that the photoresponse is linked with the incident light. The photoresponse is stable with no appreciable change in the magnitude of photocurrent over all the on/off cycles in the measurement. Interestingly, the symmetric transistors show a positive photoresponse as other normal photodetectors (Figure S4, Supporting Information). The abnormal negative photoresponse from MoS_2/DWCNT asymmetric transistors has been demonstrated before.[24] It is explained as that MoS_2 works as an efficient light absorber in the visible range, and subsequent electron transfer to DWCNT compensates intrinsic p-type doping of DWCNTs.[27] Besides, the photoresponsivity of the asymmetric device is relatively small, only ≈0.6 A W^{-1}, which is far behind those of the 2D heterostructures,[28–31] such as 20.5 A W^{-1} of WSe_2/Bi_2Te_3, 36 A W^{-1} of $MoS_2/MoSe_2$, and 108.7 A W^{-1} of WSe_2/SnS_2.[32–34] To further improve the detection performance, various strategies can be applied, such as, selecting higher photoresponse 1D materials (such as GaAs nanowire, semiconducting carbon nanotubes, and conductive polymer nanowires), and designing a novel device structure (such as pre-patterned 1D materials). It is believed that the mixed-dimensional 1D/2D heterostructures are a promising candidate for high-performance solid-state electronic and optoelectronic devices with unique properties (e.g., symmetry breaking[35] and giant optical and electronic anisotropy[36]). Further, 1D nanomaterials can be integrated with 2D components, serving as interconnectors or conducting channels for large-scale integrated circuits.[37] In addition, our demonstrated simple and efficient fabrication method for mixed-dimensional 1D/2D heterostructures can be applied to various optical structures (e.g., silicon waveguides, resonators) to improve the device performance.

3. Conclusion

In conclusion, we have reported a MoS_2/DWCNT mixed-dimensional heterostructure synthesized by sulfurating a non-volatile salt, Na_2MoO_4, on a substrate with the DWCNT film. The MoS_2/DWCNT heterostructures have a lateral size of 10–20 μm and are constituted of DWCNTs on monolayer MoS_2 which is certificated by the cross-sectional TEM morphology. The confirmed stacking order of MoS_2/DWCNT heterostructure fills in the deficiencies of previous studies and might lead to new ideas in the synthesis of mixed-dimensional heterostructures. The resulting heterostructure shows a p-type semiconductor property and an abnormal negative photoresponse as the photodetector, which can be applied as high-performance functional devices.

4. Experimental Section

Na_2MoO_4 (99.9%, Sigma-Aldrich) was used as purchased. Si substrates with a 285 nm thick SiO_2 were purchased from Siegert Wafer and cleaned with acetone and *i*-propanol, following with O_2 plasma treatment before use. The growth occurred in a homemade two-zone tube furnace. N_2 (99.995%, Agar) was chosen as carrier gas.

Raman spectra were measured using a WITec alpha300 RA+ system with a 532 nm continuous wave laser. AFM topographic images were measured by Bruker AFM Dimension Icon. SEM images were taken from Zeiss Sigma VP. The specimen for cross-sectional TEM was manufactured by JEOL JIB-4700F and was observed by JEOL JEM-2200FS(Cs-corrected HR-TEM). Electrical measurements were carried out in a scanning near-field optical microscope (WITec alpha300 RA+) system with two sourcemeters (Keithley 2400 and 2401) at room temperature under ambient conditions.

Supporting Information

Supporting Information is available from the Wiley Online Library or from the author.

Acknowledgements

The authors thank the provision of facilities and technical support by Aalto University at OtaNano-Micronova Nanofabrication Centre and OtaNano-Nanomicroscopy Center (Aalto-NMC). The authors also acknowledge support from the Academy of Finland (Grant Nos. 314810, 333982, 336144, 336818, and 340932), the Academy of Finland Flagship Programme (Grant No. 320167, PREIN), the European Union's Horizon 2020 Research and Innovation Program (Grant No. 820423, S2QUIP; 965124, FEMTOCHIP), the EU H2020-MSCA-RISE-872049 (IPN-Bio), and the European Research Council (Grant No. 834742).

Conflict of Interest

The authors declare no conflict of interest.

Data Availability Statement

The data that support the findings of this study are available in the supplementary material of this article.

Keywords

chemical vapor deposition, double-wall carbon nanotube, mixed-dimensional heterostructure, molybdenum disulfide, negative photoresponse, stacking order

Received: January 24, 2022
Revised: February 11, 2022
Published online:

[1] K. S. Novoselov, A. K. Geim, S. V. Morozov, D. Jiang, Y. Zhang, S. V. Dubonos, I. V. Grigorieva, A. A. Firsov, *Science* **2004**, *306*, 666.
[2] A. C. Ferrari, F. Bonaccorso, V. Fal'Ko, K. S. Novoselov, S. Roche, P. Bøggild, S. Borini, F. H. L. Koppens, V. Palermo, N. Pugno, J. A. Garrido, R. Sordan, A. Bianco, L. Ballerini, M. Prato, E. Lidorikis, J. Kiviojia, C. Marinelli, T. Ryhänen, A. Morpurgo, J. N. Coleman, V. Nicolosi, L. Colombo, A. Fert, M. Garcia-Hernandez, A. Bachtold, G. F. Schneider, F. Guinea, C. Dekker, M. Barbone, et al., *Nanoscale* **2015**, *7*, 4598.
[3] K. S. Novoselov, A. Mishchenko, A. Carvalho, A. H. Castro Neto, *Science* **2016**, *353*, 6298.
[4] D. Jariwala, T. J. Marks, M. C. Hersam, *Nat. Mater.* **2017**, *16*, 170.
[5] J. Jang, Y. Lee, J.-Y. Yoon, H. H. Yoon, J. Koo, J. Choe, S. Jeon, J. Sung, J. Park, W. C. Lee, H. Lee, H. Y. Jeong, K. Park, K. Kim, *Nano Lett.* **2018**, *18*, 6214.

[6] D. Zhao, Y. Chen, W. Jiang, X. Wang, J. Liu, X. Huang, S. Han, T. Lin, H. Shen, X. Wang, W. Hu, X. Meng, J. Chu, J. Wang, *Adv. Electron. Mater.* **2021**, *7*, 2001066.
[7] A. Jorio, R. Saito, *J. Appl. Phys.* **2021**, *129*, 021102.
[8] S. Manzeli, D. Ovchinnikov, D. Pasquier, O. V. Yazyev, A. Kis, *Nat. Rev. Mater.* **2017**, *2*, 17033.
[9] Z. Hu, Z. Wu, C. Han, J. He, Z. Ni, W. Chen, *Chem. Soc. Rev.* **2018**, *47*, 3100.
[10] R. Frisenda, A. J. Molina-Mendoza, T. Mueller, A. Castellanos-Gomez, H. S. Van Der Zant, *Chem. Soc. Rev.* **2018**, *47*, 3339.
[11] Q. Zhang, N. Wei, P. Laiho, E. I. Kauppinen, *Top. Curr. Chem.* **2017**, *375*, 90.
[12] Q. Zhang, W. Zhou, X. Xia, K. Li, N. Zhang, Y. Wang, Z. Xiao, Q. Fan, E. I. Kauppinen, S. Xie, *Adv. Mater.* **2020**, *32*, 2004277.
[13] T. L. Phan, Q. A. Vu, Y. R. Kim, Y. S. Shin, I. M. Lee, M. D. Tran, J. Jiang, D. H. Luong, L. Liao, Y. H. Lee, W. J. Yu, *ACS Appl. Mater. Interfaces* **2019**, *11*, 25516.
[14] L. Li, Y. Guo, Y. Sun, L. Yang, L. Qin, S. Guan, J. Wang, X. Qiu, H. Li, Y. Shang, Y. Fang, *Adv. Mater.* **2018**, *30*, 1706215.
[15] S. Li, Y.-C. Lin, W. Zhao, J. Wu, Z. Wang, Z. Hu, Y. Shen, D.-M. Tang, J. Wang, Q. Zhang, H. Zhu, L. Chu, W. Zhao, C. Liu, Z. Sun, T. Taniguchi, M. Osada, W. Chen, Q.-H. Xu, A. T. S. Wee, K. Suenaga, F. Ding, G. Eda, *Nat. Mater.* **2018**, *17*, 535.
[16] S. Li, Y.-C. Lin, X.-Y. Liu, Z. Hu, J. Wu, H. Nakajima, S. Liu, T. Okazaki, W. Chen, T. Minari, Y. Sukuma, K. Tsukagoshi, K. Suenaga, T. Taniguchi, M. Osada, *Nanoscale* **2019**, *11*, 16122.
[17] S. Li, *iScience* **2021**, *24*, 103229.
[18] X. Bai, S. Li, S. Das, L. Du, Y. Dai, L. Yao, R. Raju, M. Du, H. Lipsanen, Z. Sun, *Nanoscale* **2021**, *13*, 4537.
[19] Q. Zhang, J.-S. Nam, J. Han, S. Datta, N. Wei, E.-X. Ding, A. Hussain, S. Ahmad, V. Skakalova, A. T. Khan, Y.-P. Liao, M. Tavakkoli, B. Peng, K. Mustonen, D. Kim, I. Chung, S. Maruyama, H. Jiang, I. Jeon, E. I. Kauppinen, *Adv. Funct. Mater.* **2021**, *32*, 2103397.
[20] H. Li, Q. Zhang, C. C. R. Yap, B. K. Tay, T. H. T. Edwin, A. Olivier, D. Baillargeat, *Adv. Funct. Mater.* **2012**, *22*, 1385.
[21] D. M. Seo, J.-H. Lee, S. Lee, J. Seo, C. Park, J. Nam, Y. Park, S. Jin, S. Srivastava, M. Kumar, Y. M. Jung, K.-H. Lee, Y.-j. Kim, S. Yoon, Y. L. Kim, P. M. Ajayan, B. K. Gupta, M. G. Hahm, *ACS Photonics* **2019**, *6*, 1379.
[22] Z. Li, S.-W. Chang, C.-C. Chen, S. B. Cronin, *Nano Res.* **2014**, *7*, 973.
[23] X.-X. Li, Z.-Q. Fan, P.-Z. Liu, M.-L. Chen, X. Liu, C.-K. Jia, D.-M. Sun, X.-W. Jiang, Z. Han, V. Bouchiat, J.-J. Guo, J.-H. Chen, Z.-D. Zhang, *Nat. Commum.* **2017**, *8*, 970.
[24] V. T. Nguyen, W. Yim, S. J. Park, B. H. Son, Y. C. Kim, T. T. Cao, Y. Sim, Y.-J. Moon, V. C. Nguyen, M.-J. Seong, S.-K. Kim, Y. H. Ahn, S. Lee, J.-Y. Park, *Adv. Funct. Mater.* **2018**, *28*, 1802572.
[25] L.-M. Peng, Z. Zhang, S. Wang, *Mater. Today* **2014**, *17*, 433.
[26] L. Wang, L. Chen, S. L. Wong, X. Huang, W. Liao, C. Zhu, Y.-F. Lim, D. Li, X. Liu, D. Chi, K.-W. Ang, *Adv. Electron. Mater.* **2019**, *5*, 1900393.
[27] W. Su, L. Jin, D. Huo, L. Yang, *Opt. and Quantum Electron.* **2017**, *49*, 197.
[28] M. Long, P. Wang, H. Fang, W. Hu, *Adv. Funct. Mater.* **2019**, *29*, 1803807.
[29] F. H. L. Koppens, T. Mueller, P. Avouris, A. C. Ferrari, M. S. Vitiello, M. Polini, *Nat. Nanotechnol.* **2014**, *9*, 780.
[30] H. Xue, Y. Dai, W. Kim, Y. Wang, X. Bai, M. Qi, K. Halonen, H. Lipsanen, Z. Sun, *Nanoscale* **2019**, *11*, 3240.
[31] H. Xue, Y. Wang, Y. Dai, W. Kim, H. Jussila, M. Qi, J. Susoma, Z. Ren, Q. Dai, J. Zhao, K. Halonen, H. Lipsanen, X. Wang, X. Gan, Z. Sun, *Adv. Funct. Mater.* **2018**, *28*, 1804388.
[32] H. Liu, X. Zhu, X. Sun, C. Zhu, W. Huang, X. Zhang, B. Zheng, Z. Zou, Z. Luo, X. Wang, D. Li, A. Pan, *ACS Nano* **2019**, *13*, 13573.
[33] F. Li, B. Xu, W. Yang, Z. Qi, C. Ma, Y. Wang, X. Zhang, Z. Luo, D. Liang, D. Li, Z. Li, A. Pan, *Nano Res.* **2020**, *13*, 1053.
[34] T. Yang, B. Zheng, Z. Wang, T. Xu, C. Pan, J. Zou, X. Zhang, Z. Qi, H. Liu, Y. Feng, W. Hu, F. Miao, L. Sun, X. Duan, A. Pan, *Nat. Commun.* **2017**, *8*, 1906.
[35] L. Du, T. Hasan, A. Castellanos-Gomez, G.-B. Liu, Y. Yao, C. N. Lau, Z. Sun, *Nat. Rev. Phys.* **2021**, *3*, 193.
[36] L. Du, Y. Zhao, L. Wu, X. Hu, L. Yao, Y. Wang, X. Bai, Y. Dai, J. Qiao, M. G. Uddin, X. Li, J. Lahtinen, X. Bai, G. Zhang, W. Ji, Z. Sun, *Nat. Commun.* **2021**, *12*, 4822.
[37] P.-Y. Huang, J.-K. Qin, C.-Y. Zhu, L. Zhen, C.-Y. Xu, *J. Phys. Condens. Matter* **2021**, *33*, 493001.